Separation and Purification Technology 330 (2024) 125558

Contents lists available at ScienceDirect

Separation and Purification Technology

journal homepage: www.elsevier.com/locate/seppur

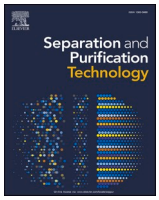

Microwave-assisted synthesis of metal–organic frameworks UiO-66 and MOF-808 for enhanced CO_2/CH_4 separation in PIM-1 mixed matrix membranes

Mohamed Yahia [a,b,c,*], Luis A. Lozano [d], Juan M. Zamaro [d], Carlos Téllez [a,b], Joaquín Coronas [a,b,*]

[a] Instituto de Nanociencia y Materiales de Aragón (INMA), CSIC-Universidad de Zaragoza, Zaragoza 50018, Spain
[b] Chemical and Environmental Engineering Department, Universidad de Zaragoza, Zaragoza 50018, Spain
[c] Chemistry Department, Faculty of Science, Helwan University, Cairo 11795, Egypt
[d] Instituto de Investigaciones en Catálisis y Petroquímica, Facultad de Ingeniería Química, Universidad Nacional del Litoral (FIQ-UNL), Argentina

ARTICLE INFO

Editor: Zhaoxiang Zhong

Keywords:
Polymers of intrinsic microporosity (PIMs)
Mixed matrix membrane (MMM)
Zr-metal–organic framework (MOF)
Microwave-assisted synthesis
CO_2/CH_4 separation

ABSTRACT

This study presents a sustainable microwave-assisted synthesis, based on the use of acetone and a water/acetic acid mixture instead of typical harmful DMF, to fabricate Zr-metal–organic frameworks (MOFs) UiO-66 and MOF-808 as fillers in a PIM-1 matrix for gas separation application. The mixed matrix membranes (MMMs) were prepared with varying loadings (2.5–10 wt%) of MOFs. The physicochemical properties (^{1}H NMR, FTIR, XRD, N_2 adsorption, TGA and SEM) of the resulting PIM-1, MOFs and MMMs were analyzed. The CO_2/CH_4 separation performance and membrane aging characteristics of the MMMs were evaluated. The incorporation of MOF fillers significantly improved CO_2 permeability and CO_2/CH_4 selectivity, attributed to their CO_2-philicity and narrow pore size (UiO-66 ≈ 0.6 nm and MOF-808 ≈ 1.8 nm). The MMMs with higher filler loadings (7.5 and 10 wt%) exhibited the most favorable separation performance. Due to the better crystallinity and textural properties, MOF-808 produced the best separation results at 10 wt% filler loading (a CO_2/CH_4 separation selectivity of 16.2 at 9090 Barrer of CO_2 permeability). Aging led to a decrease in CO_2 permeability but a slight increase in CO_2/CH_4 selectivity for all MMMs. Overall, the study highlights the potential of PIM-1/UiO-66 and PIM-1/MOF-808 MMMs as efficient materials for (CO_2/CH_4) separation comparing with the pristine PIM-1.

1. Introduction

The existence of carbon dioxide (CO_2) is widespread, frequently seen in natural gas, biogas, and produced when burning fossil fuels or converting coal [1]. Regarding methane (CH_4) gas streams, it is essential to remove CO_2 for improving their quality and performance, particularly for biogas production prior to injecting into distribution systems [1,2]. This is crucial to prevent a decrease in the energy value, corrosion and harmful effects on the compression and transportation characteristic of the gas. Therefore, the efficient and cost-effective separation of CO_2 is extremely required [1,2]. Various traditional industrialized techniques such as cryogenic, absorption, adsorption and membrane separation have been employed for CO_2 capture and separation [3–6]. Among these methods, the separation technology based on membranes has been practically applied and offers several advantages over other traditional processes [3–6]. These advantages include high productivity, scalability, processability, and a small footprint, making it an attractive option for CO_2 separation [1,2]. As a result, there is a high require for membrane materials that demonstrate extreme selectivity, to minimize methane losses, and high permeability, to reduce manufacturing costs and physical footprint [7–9].

Mixed matrix membranes (MMMs) offer a promising prospect to merge the best features of polymeric organic materials, which are easily processable, with the outstanding transport performing of certain fillers [10,11]. The primary goal of developing these innovative materials is to create membranes with superior permeability and selectivity for gas separation applications that exceed the so-called Robeson-upper bound line [4,5,12]. In general, the combination of inorganic nano-fillers into a polymer structure can alter permeability either by enabling a molecular sieving, changing solubility or generating a barrier effect or disordering

* Corresponding authors.
E-mail addresses: mohamed.yahia@science.helwan.edu.eg (M. Yahia), coronas@unizar.es (J. Coronas).

https://doi.org/10.1016/j.seppur.2023.125558
Received 28 July 2023; Received in revised form 6 October 2023; Accepted 29 October 2023
Available online 3 November 2023

of the polymer chains [13,14]. However, the fabrication of MMMs faces a significant challenge in achieving proper dispersibility of inorganic nano-fillers in the polymer architecture. The existence of fillers in high concentrations leads to diminish the gas separation performing and membrane mechanical stability [15,16]. Moreover, poor separation selectivity is a potential issue in MMMs when the nano-filler and polymer are incompatible, creating networks at their interface that alllow gas transport through low selective Knudsen diffusion [17,18].

Polymers of intrinsic microporosity (PIMs) have attracted a great attention due to their good gas transfer characteristics, particularly highly permeability and reasonable selectivity. The inter-connectivity of micro-cavities and the spiro-bisindane moiety, which creates considerable steric hindrance, contributes to a high fractional free volume (FFV) and rigidity in the polymer chains [19–21]. PIM-1 is the most studied microporous polymer among the PIMs due to its easily solubility, excellent physio-chemical and thermal stability and excellent properties for CO_2/CH_4 separation with selectivity in the ca. 12–18 range. Additionally, PIM-1 exhibits a remarkable adsorption capability for smaller molecules and is useful for catalysis application [21–23]. The selection process for both polymer and filler components holds paramount importance as it influences the morphology and overall efficacy of MMMs in gas separation [11,15]. By selecting the appropriate combination of polymer and filler, it is possible to produce advanced membranes with an exceptional gas separation performance [15].

Metal-organic frameworks-MOFs are a novel group of nano-porous materials that are constructed by linking metal-clusters with organic units [24] giving rise to porosity with a specific size and shape [25]. Due to their crystallinity, microporosity and specific interaction with molecules like CO_2, MOFs can lead as filler in a polymer matrix to achieving improvements in the solubility and/or diffusivity of the targeted gas molecules, as well as mitigating the effects of physical aging or enhancing plasticization resistance [26]. Compared to inorganic fillers, MOFs have good compatibility with polymers owing to its organic nature and a greater pore volume at a lower density [27,28]. MOFs can be tailored to have pre-defined cage dimensions and functionalized ligands, which can increase their affinity for both the phase of organic polymer and transported gases. This supports MOFs as an appealing option for separation applications [14,29]. It is estimated that MOF fillers will further enhance the performance of the PIM-MMMs [18,30,31].

As compared to other fillers, Zr-based MOFs, when embedded in MMMs, exhibit some of the most noteworthy CO_2/CH_4 permeability and selectivity [32]. This exceptional performance can be ascribed to the electrostatic potential and acid-base Lewis's interactions existing at the Zr-MOF carboxylate type ligands, which possess a significant affinity for CO_2 quadrupole moment when compared to CH_4 [33,34]. Moreover, CO_2 has a higher diffusivity than CH_4 owing to the CO_2 small kinetic diameter (0.33 nm) comparing to that of CH_4 (0.38 nm), and the latter is steric hindered by the Zr-MOFs microporous structure [14]. The CO_2/CH_4 separation efficiency of PIM-1/MOF MMMs is significantly influenced by how MOFs are incorporated into the polymer architecture, depending on various factors such as their particle size [35] and shape [36], MOFs structure and surface modifications [37,38], MOF loading and the conditions of membrane synthesis, including temperature and method [29,34,39–41].

The UiO-66 and MOF-808 are types of Zr-based MOFs currently being explored for gas separation and capture [11,42–45]. These MOFs are created by using carboxylate-type linkers and Zr clusters to form highly porous frameworks. One of their notable advantages is the ability to incorporate different linkers to tailor the interaction between the MOFs and the polymer matrix, which is an important factor affecting the gas transport properties of MMMs. Several studies have examined the transport properties of various isoreticular-UiO-66-based MMMs and found that their CO_2 permeability and selectivity can be improved by incorporating various kinds of isoreticular UiO-66 in the corresponding MMMs [42]. For instance, the existence of $–NH_2$ groups in UiO-66-NH_2 resulted in a reduced CO_2 permeability and a little rising in CO_2/CH_4 selectivity [11,42–44]. Computational studies have also shown that modifying the functional groups of UiO-66 ligands can enhance the CO_2/CH_4 adsorption selectivity [44].

The addition of MOF fillers to membrane materials greatly enhanced the ability of CO_2 to pass through and be selectively separated. This improvement is mainly due to the porous structure of the created MOFs, which makes it easier for CO_2 to move through. Additionally, the active functional groups in the MOF ligands, particularly the carboxylate groups based on zirconium, make the MOF particles attract CO_2 more strongly and also have a good fit with the PIM-1 polymer. These interactions between the polymer and filler materials create more paths for CO_2 to travel through the membranes, ultimately leading to better selectivity in separating CO_2 from other gases.

Microwave-assisted synthesis of MOFs offers several notable advantages. Firstly, it provides a rapid heating rate, enabling significantly reduced synthesis times, sometimes taking only a few seconds. This characteristic enhances energy efficiency, leading to substantial reductions in energy consumption. Secondly, the synthetic process can be easily controlled upon deactivation of the microwave power. Lastly, this method is environmentally friendly, resulting in substantial reductions in pollution generation [46]. In this study, a sustainable method using microwave-assisted synthesis was employed to obtain UiO-66 and MOF-808 by replacing in turn N,N-dimethylformamide (DMF) with an acetone and water-based reaction mixture and performing the synthesis at relatively low temperatures. The physico-chemical characteristics of the resulting Zr-MOFs were analyzed, and the most promising materials were selected for incorporation into a PIM-1 matrix at varying loadings up to 10 wt%. The resulting PIM-1/MOF MMMs were evaluated for their CO_2/CH_4 separation performance and membrane aging at 35 °C, as well as other relevant properties. The main novelty of this study lies in the demonstration of the feasibility of synthesizing two different Zr-based MOFs, namely MOF-808 and UiO-66, using an environmentally microwave-assisted method with acetone as solvent instead of typical harmful DMF. These synthesized MOF share a common chemistry characterized by Zr-based carboxylate ligands but differ significantly in terms of their pore sizes, with UiO-66 possessing pores of approximately 0.6 nm and MOF-808 exhibiting larger pores of around 1.8 nm. Furthermore, this research indicates the potential of MMMs composed of PIM-1/UiO-66 and PIM-1/MOF-808 as highly efficient materials for the separation of mixed (CO_2/CH_4) gases when compared to pristine PIM-1.

2. Experimental

2.1. Materials

For synthesizing UiO-66, benzene-dicarboxylic acid (BDC) (Aldrich, 98.0%), $ZrCl_4$ (Aldrich, 98.0%) and acetone (Cicarelli, 99.0%) as solvent were utilized. Additionally, the synthesis of MOF-808 involved using benzene tricarboxylic acid (BTC) (Aldrich, 95.0%), $ZrCl_4$ (Aldrich, 98.0%), with glacial acetic acid and deionized water as solvents. All the chemical reagents were utilized without any additional purification. PIM-1 was synthesized using reagent grade chemicals including potassium carbonate anhydrous (K_2CO_3), methanol (MeOH), N-methyl-pyrrolidone (NMP), chloroform ($CHCl_3$), and toluene, from Sigma-Aldrich with a purity greater than 99%. Tetrafluoroterephthalonitrile (TFTPN) and tetramethyl-1,1′-spirobiindane-5,5′,6,6′-tetraol (TTSBI) were acquired from Sigma-Aldrich; the first one was purified by recrystallization in MeOH, while the later was refined by sublimation at (150 °C).

2.2. Methodology

2.2.1. Synthesis of polymer PIM-1 and MOFs UiO-66 and MOF-808

PIM-1 (MW ≈ 74 kDa, polydispersity index (PDI) = 1.85, as determined by GPC-MALS) was synthesized using a previous protocol [14,20,47]. In the synthesis process, TFTPN and TTSBI (both at 0.01 mol) were combined with anhydrous K_2CO_3 (0.03 mol), NMP (20 mL),

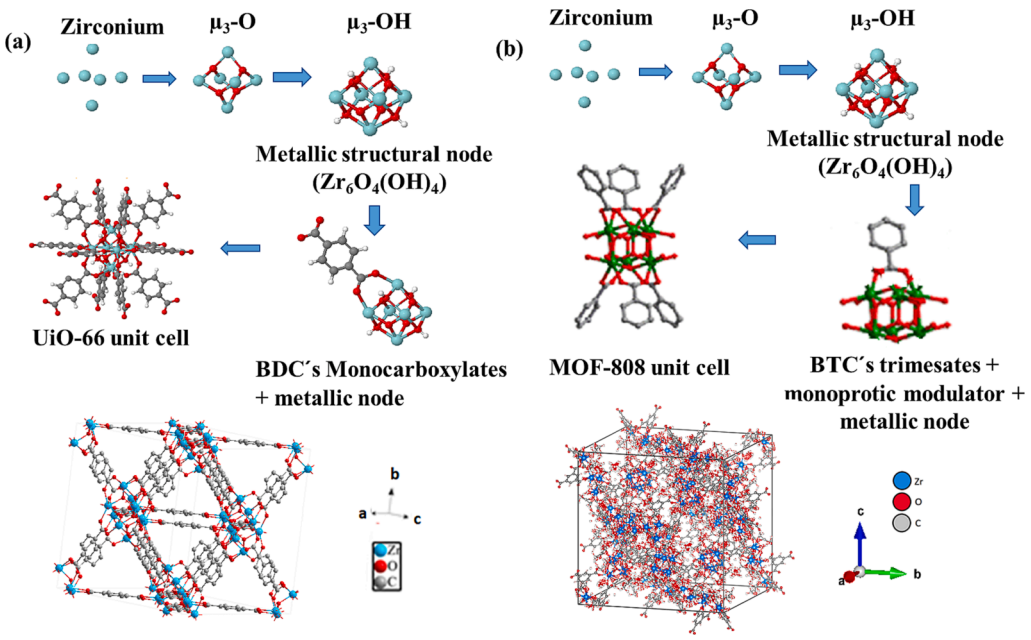

Fig. 1. (a) Top: UiO-66 formation units. Down: Simulated unit cell from CCDC file 733458 using Diamond 3.2 software. (b) Top: MOF-808 formation units. Down: MOF-808 unit cell simulated from CCDC file 1002672 using the free software Vesta.

and toluene (10 mL) in a nitrogen-protected three-necked flask with continuous stirring. The mixture was refluxed at 160 °C for 4 h, yielding a thick solution that was then precipitated using MeOH. The resulting polymer was dried, redissolved in $CHCl_3$, re-precipitated with MeOH, and finally dried overnight at 80 °C.

To synthesize UiO-66, a DMF-free protocol was utilized [48] and the reaction was performed out under microwave heating process that were previously optimized [49]. The procedure involved mixing (BDC and $ZrCl_4$) with acetone under magnetic stirring for 25 min to produce a homogeneous mixture of 70 mL with a molar ratio of BDC:$ZrCl_4$:acetone = 1:1:1622. The mixture was then treated under stirring for 6 h at 80 °C in an autoclave using a Milestone flexiWAVE microwave oven (220 V, 50 Hz). For the synthesis of MOF-808 [50], a similar procedure was used by replacing the carboxylate ligand (BDC with BTC), the mixture of reagents (BTC and $ZrCl_4$) and solvents was homogenized using magnetic stirring. The molar ratio of BTC:$ZrCl_4$:acetic acid:water was maintained at 0.333:1:44:138, as well as the solvent volume of 20 mL (see the supplementary information for additional details).

2.2.2. Membrane fabrication

PIM-1/UiO-66 and PIM-1/MOF-808 MMMs with 2.5–10 wt% MOF crystals were prepared as follows: first, PIM-1 was solubilized in $CHCl_3$. Next, MOF dispersions were created by sonication of UiO-66 and MOF-808 in $CHCl_3$ using an ultrasonic bath for 1 h. The solution of PIM-1 and MOF dispersion were mixed and stirred for 3 h more. Finally, the suspensions were cast into Petri glass dishes allowing 3 days for completing the evaporation of solvent at ambient temperature. Before membrane testing (bare PIM-1 and MMMs), the membranes after drying were immersed for 30 min in methanol, dried overnight in oven under vacuum at 60 °C and stored in a dark place at ambient temperature.

2.2.3. PIM-1, MOFs and membrane characterization

A Bruker Avance III 400 spectrometer (Bruker, Billerica, MA, USA) operating at 400 MHz proton frequency and 25 °C was used to conduct ^1H NMR with $CDCl_3$ as an internal reference. Gel permeation chromatography (GPC) combined with multi angle light scattering (MALS) detection was conducted to analyze the PIM-1 molecular weight. The Bruker Vertex 70 FTIR spectrometer, which included a DTGS detector and a Golden Gate diamond ATR accessory, was used to carry out Fourier transform infrared spectroscopy (FTIR). Using a Mettler Toledo TGA/STDA 851e, thermogravimetric analyses (TGA) and differential thermogravimetry (DTA) were conducted.

To analyze the membrane and MOF crystallinity, X-ray diffraction (XRD) was performed using a Panalytical Empyrean equipment with CuKα radiation (λ = 0.154 nm), scanning between 5° to 40° (2·theta) at a rate of $0.03°\cdot s^{-1}$. Micromeritics Tristar 3000 was used to record the N_2 isotherms at −196 °C. The specific surface area (SSA) of the porous materials was calculated using the Brunauer-Emmett-Teller (BET) method. Scanning electron microscope (SEM) images were achieved for the membranes using a FEI Inspect F50 model operating at 10 kV. The membrane thickness was measured at 5–6 different positions along the membrane using micrometer scale, the measured thickness value was around 100–200 μm, (see the supplementary information for additional details).

2.2.4. Gas permeation measurements

The used set-up for the CO_2/CH_4 mixture separation is as follows [29]: a membrane circle was cut and put in a design module composed of dual stainless steel parts and a 316LSS macro-porous disc support with a pore-size (20 μm). The membranes, which had an area of 2.12 cm^2, were clamped inside the permeation module by Viton o-rings. The temperature of the membrane was regulated at 35 °C by placing the module of permeation in an oven (Memmert). Gas separation was performed by feeding a 50/50 $cm^3(STP)\cdot min^{-1}$ CO_2/CH_4 mixture at 3 bar. The membrane permeate side was purged at atmospheric pressure (ca. 1 bar) with 2 $cm^3(STP)\ min^{-1}$ of He. All these gas streams were regulated by mass-flow controllers ·(Alicat). An Agilent 990 micro-gas chromatograph continuously evaluated the CO_2 and CH_4 concentrations in the permeate stream. After reaching steady state (after ca. 3 h), CO_2 and CH_4 permeabilities were recorded in Barrer (10^{-10} $cm^3(STP)\cdot cm\cdot cm^{-2}\cdot s^{-1}\cdot cmHg^{-1}$), as the flux divided by the membrane area and partial pressure and multiplied by the thickness of the membrane. The CO_2/CH_4 selectivity was determined as the corresponding permeabilities ratio. The formulas used to calculate the permeability (Eq.1) and selectivity (Eq.2) are as follows [51,52]:

$$P_{gas} = \frac{Flux_{gas}\ (cm^3(STP)\cdot cm^{-2}\cdot s^{-1})\cdot Thickness\ (cm)}{\Delta P_{gas}\ (cmHg)} \quad (1)$$

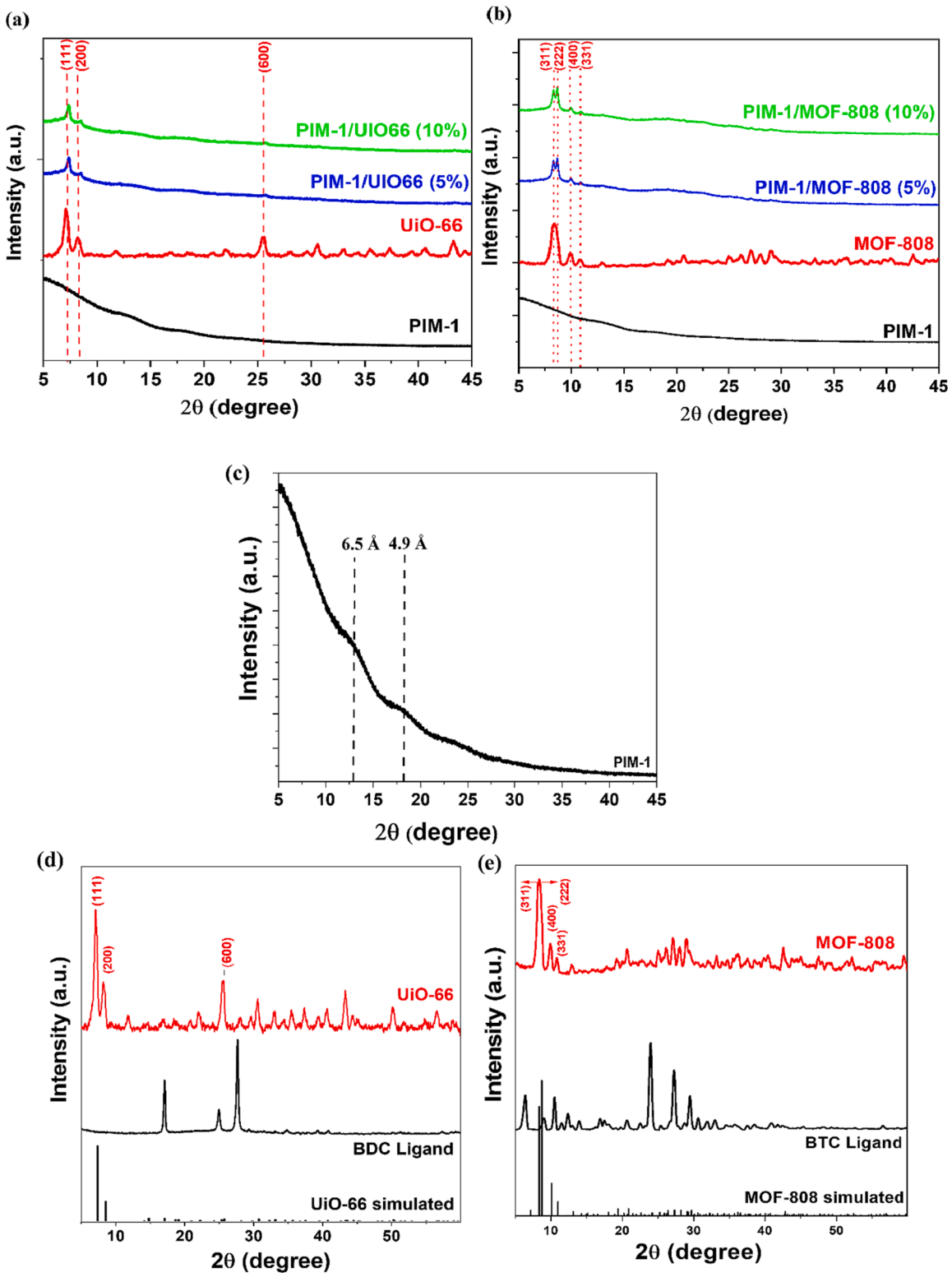

Fig. 2. XRD patterns of: (a) PIM-1 (powder), UiO-66 and PIM-1/UiO-66 MMMs, (b) PIM-1 (powder), MOF-808 and PIM-1/MOF-808 MMMs, (c) PIM-1 pristine membrane, and (d, e) UiO-66 and MOF-808 with their simulated patterns from their corresponding crystallographic data (CCDC files 733458 and 1002672).

$$\alpha = \frac{P_{CO2}}{P_{CH4}} \tag{2}$$

To investigate the influence of physical aging on membrane performance, the membranes have been stored for 45 days in a dried desiccator to prevent moisture. Afterward, gas permeation tests were conducted on the aged membranes without any methanol treatment. To ensure accurate results and errors, each membrane was measured five times before and after the aging period.

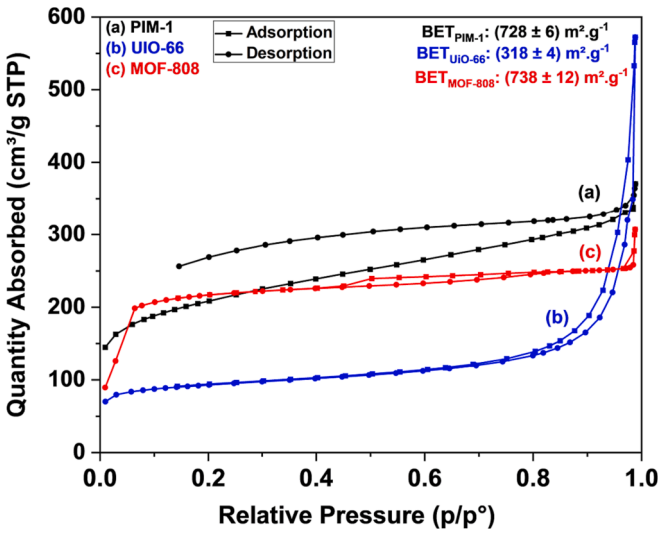

Fig. 3. N_2 isotherms at -196 °C for PIM-1 and MOFs UiO-66 and MOF-808 with the corresponding BET specific surface areas.

3. Results and discussion

3.1. Preparation and characterization of MOFs and MMMs

Fig. 1a represents the formation units of UiO-66 and the corresponding simulated unit cell. UiO-66 is fabricated of a group of 6 Zr-atoms linked to oxygen atoms and hydroxyl groups. These units are linked together by BDC moities forming the unit cell. Multiple unit cells connect to create the unique three-dimensional structure of UiO-66. In meanwhile Fig. 1b shows the formation units of MOF-808 and its simulated unit cell. MOF-808 also has the same metal cluster than UiO-66, consisting of $Zr_6O_4(OH)_4$. This cluster is connected by BTC ligands and the monoprotic modulator to form the unit cell. Like UiO-66, multiple unit cells join together to form the distinct three-dimensional arrangement of MOF-808. Crystallographic pore sizes of UiO-66 and MOF-808 are 0.6 nm [53] and 1.8 nm [54], respectively.

The PIM-1 structure was confirmed by analyzing its ^{1}H NMR and GPC spectra, which are presented in Fig. S1. The PIM-1 pristine and PIM-1/MMMs were subjected to FTIR spectroscopy (Fig. S2) to investigate the connections between MOFs (UiO-66 and MOF-808) and PIM-1. Fig. 2 depicts the PIM-1 amorphous structure via the XRD diffractogram. The two broad peaks at 13.4° and 18.0° indicate chain-to-chain distances of 0.49 nm and 0.65 nm, respectively. These distances are related to the packing efficiency of polymer chains with a ladder and microporous architecture in PIM-1 [14,22,47]. Besides, the XRD diffractograms for UiO-66 and MOF-808 are presented in Fig. 2d and Fig. 2e, respectively. The diffraction pattern of UiO-66 displays main indexed peaks at 7.4°, 8.5° and 25.7°, which associated to the crystalline planes (1 1 1), (2 0 0) and (6 0 0), respectively, consistent with the previously published literature [11,55,56]. Similarly, the significant intensities of MOF-808 were identified, as displayed in Fig. 2b. These main signals are located at 8.4°, 8.7°, 10.1° and 11.0°, and correspond to the crystalline planes (3 1 1), (2 2 2), (4 0 0) and (3 3 1), respectively, in agreement with the published studies [55,57]. Furthermore, the XRD structures of UiO-66 and MOF-808 exhibit patterns, depicted in Fig. 2d and Fig. 2e, respectively, that have been simulated based on their crystallographic data (respective CCDC files 733458 and 1002672). These simulated patterns are consistent with the data previously published [11,55–57]. Additionally, the XRD diffractograms for PIM-1/UiO-66 and PIM-1/MOF-808 MMMs are displayed in Fig. 2a and Fig. 2b, respectively. These patterns, showing the weak signals of PIM-1, suggest that the MMMs retained the same chain-to-chain distances of 0.49 nm and 0.65 nm as in the bare polymer, demonstrating no important changes in the polymeric structure after incorporating UiO-66 or MOF-808 crystals. However, new peaks corresponding to UiO-66 and MOF-808 are observed in the diffractograms, evidencing the successful incorporation of these MOFs into the MMMs without apparent loss of crystallinity.

Furthermore, gas-sorption analysis was conducted to assess the structural rigidity and microporosity of evacuated MOFs. The obtained nitrogen adsorption and desorption isotherms, presented in Fig. 3, closely resembled the reported isotherms for these MOFs [29,48,50,58–60], providing strong evidence for their microporous nature and their capacity to adsorb and desorb N_2 gas. According to Fig. 3 and Table S1. PIM-1 has a highly BET SSA (728 $m^2 \cdot g^{-1}$) indicating its microporous properties as reported in the literature [61–63]. The combination of a type I and IV isotherm in PIM-1 implies the existence of micro and mesopores. Moreover, the prominent hysteresis observed indicates that PIM-1 contains mesopores that can only be accessed through the micropores, suggesting a regulated entrance mechanism [14,64]. Both PIM-1 and MOFs have small pore sizes and high BET SSA values, typical of nanoporous materials [65]. However, it is notified that MOF-808 has a BET SSA (738 $m^2 \cdot g^{-1}$) as high as that of PIM-1, while UiO-66 has a modest value of such parameter (318 $m^2 \cdot g^{-1}$). The obtained BET SSA values for the microwave synthesized MOFs are lower than the expected values for these materials (ca. 900–1000 $m^2 \cdot g^{-1}$) [11,55], but the obtained values for synthesized MOFs are in agreement with the previous reports in acetone-based synthesis for UiO-66 [56,66]. During the microwave-assisted synthesis, a negative thermal expansion can occur, making a thermal-induced deterioration of MOF porous structure [56]. These variations in textural properties can significantly impact on the permeating gas characteristic of MMMs containing PIM-1 and these MOFs [67]. Thus, gas transport through PIM-1 with different pore volumes, pore sizes, and BET SSA values for MOF crystals can differ significantly owing to the variations in the structure of PIM-1 microporous network [63,65,68].

Furthermore, the TGA curves were achieved in air to evaluate the

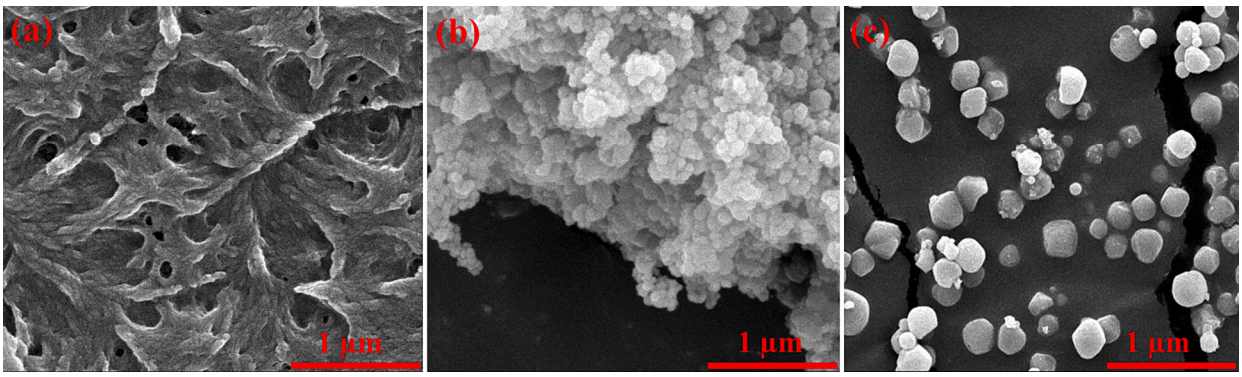

Fig. 4. SEM images for: (a) PIM-1 pristine membrane, (b) UiO-66 crystals, and (c) MOF-808 crystals.

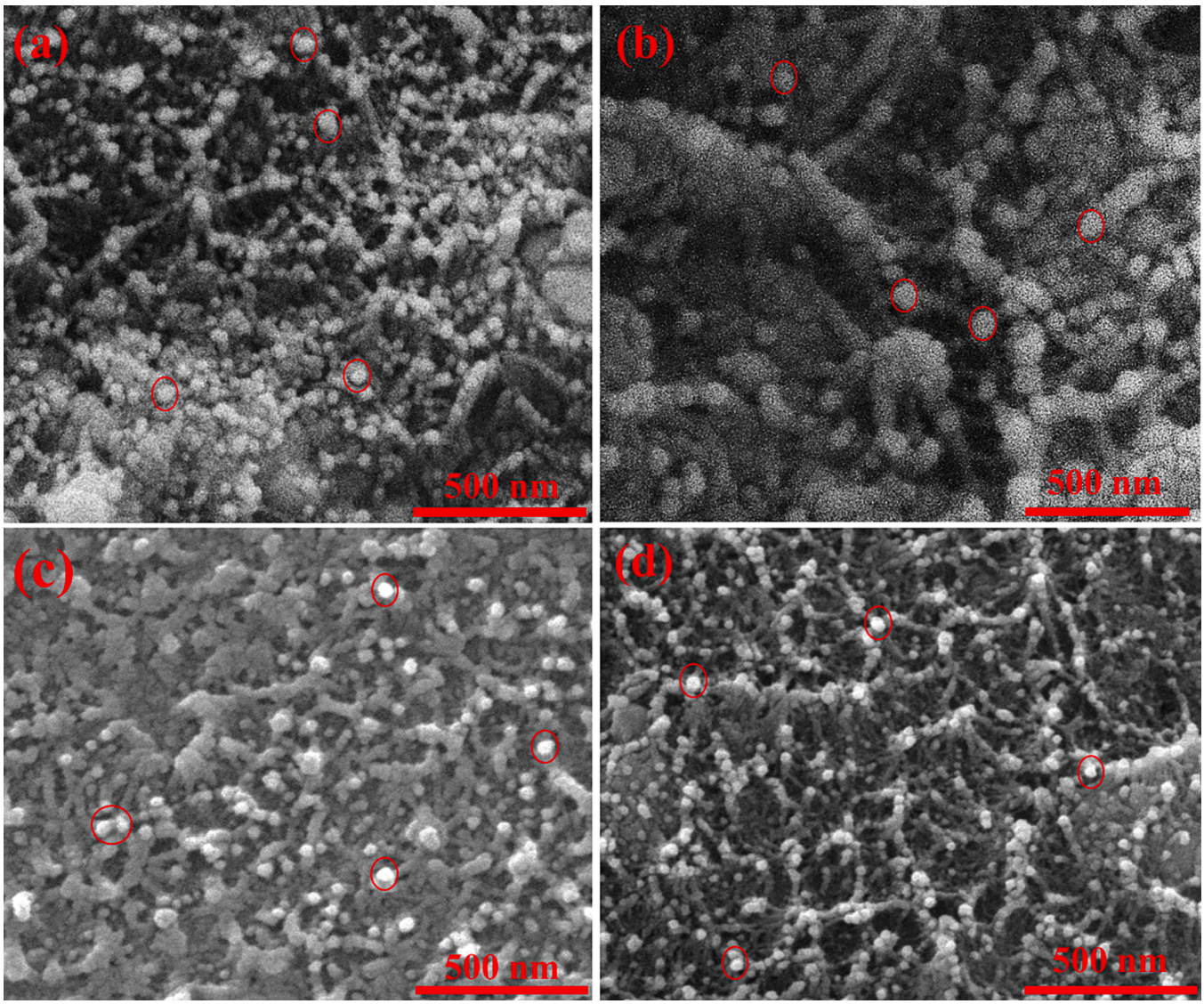

Fig. 5. SEM images for: (a) PIM-1/UiO-66 (7.5 wt%), (b) PIM-1/UiO-66 (10 wt%), (c) PIM-1/MOF-808 (7.5 wt%) and (d) PIM-1/MOF-808 (10 wt%). The UiO-66 and MOF-808 particles are marked with red circles. (For interpretation of the references to colour in this figure legend, the reader is referred to the web version of this article.)

thermal stability of pristine PIM-1 and PIM-1/MOF MMMs (see Fig. S3a and Fig. S3b in supplementary information with additional discussion). Also, as shown in Fig. S3c (supplementary information), a DTA analysis was conducted and the obtained data are aligned with the TGA findings, providing deeper insights into the thermal properties on our materials.

Fig. 4a-c displays the results corresponding to the SEM analysis carried out on PIM-1 and the MOF particles. The images provide insight into the surface morphology (the microporous character evidenced from the N_2 isotherm) of the PIM-1 matrix, similar to that reported in previous works [14,22], and the particle size of the synthesized MOFs crystals. It was evident that, as powders, UiO-66 nanoparticles exhibited agglomeration, whereas MOF-808 showed a more uniform dispersion. Also, the particle sizes range approximately from 50 to 200 nm for UiO-66 and from 100 to 300 nm for MOF-808 (see Fig. S4 in Supplementary information).

Furthermore, the SEM images shown in Fig. 5 provide insight into the structure of PIM-1/MOF MMMs with the highest loaded percentages (7.5 and 10 wt%). As observed in Fig. 5a-d, the images reveal that the fillers (UiO-66 and MOF-808) dispersed in the PIM-1 matrix exhibit similar average sizes to those observed in the corresponding powders (Fig. 4 and Fig. S4). Furthermore, the SEM analysis indicates that the formation of agglomerates of MOF nanoparticles is less prominent in the PIM-1/MOF-808 MMMs in comparison with the PIM-1/UiO-66 MMMs. This suggests a more homogeneous dispersion of MOF-808 within the bulk of the PIM-1/MOF-808 MMMs. The SEM images suggest favorable interactions between PIM-1 and MOF-808, with no visible defects or significant particle agglomerates [14,18,69]. The better interaction of MOF-808 may be due to its chemistry that presents more functional groups (BTC vs. BDC) and also to its larger pore size, both of which might promote the interaction with the polymer chains. Consequently, the PIM-1/MOF-808 MMMs exhibit the best dispersion of MOF and ultimately will demonstrate (see next section) superior CO_2/CH_4 permeability and selectivity compared to the PIM-1/UiO-66 (10 wt%) MMMs, which exhibit partial agglomeration of UiO-66 particles across the PIM-1 pristine membrane. These findings emphasize the importance of achieving a homogeneous dispersion of MOFs within PIM-1/MOF MMMs to achieve high gas perm-selectivity. Furthermore, SEM-EDS analysis was performed to gather additional details about the samples. Fig. S5 and Fig. S6 exhibit the elemental composition of UiO-66 in PIM-1/UiO-66 (10 wt%) and MOF-808 in PIM-1/MOF-808 (10 wt%), respectively. The zirconium (Zr) mapping indicates a uniform distribution of MOF particles within the surface of PIM-1/MOF MMMs,

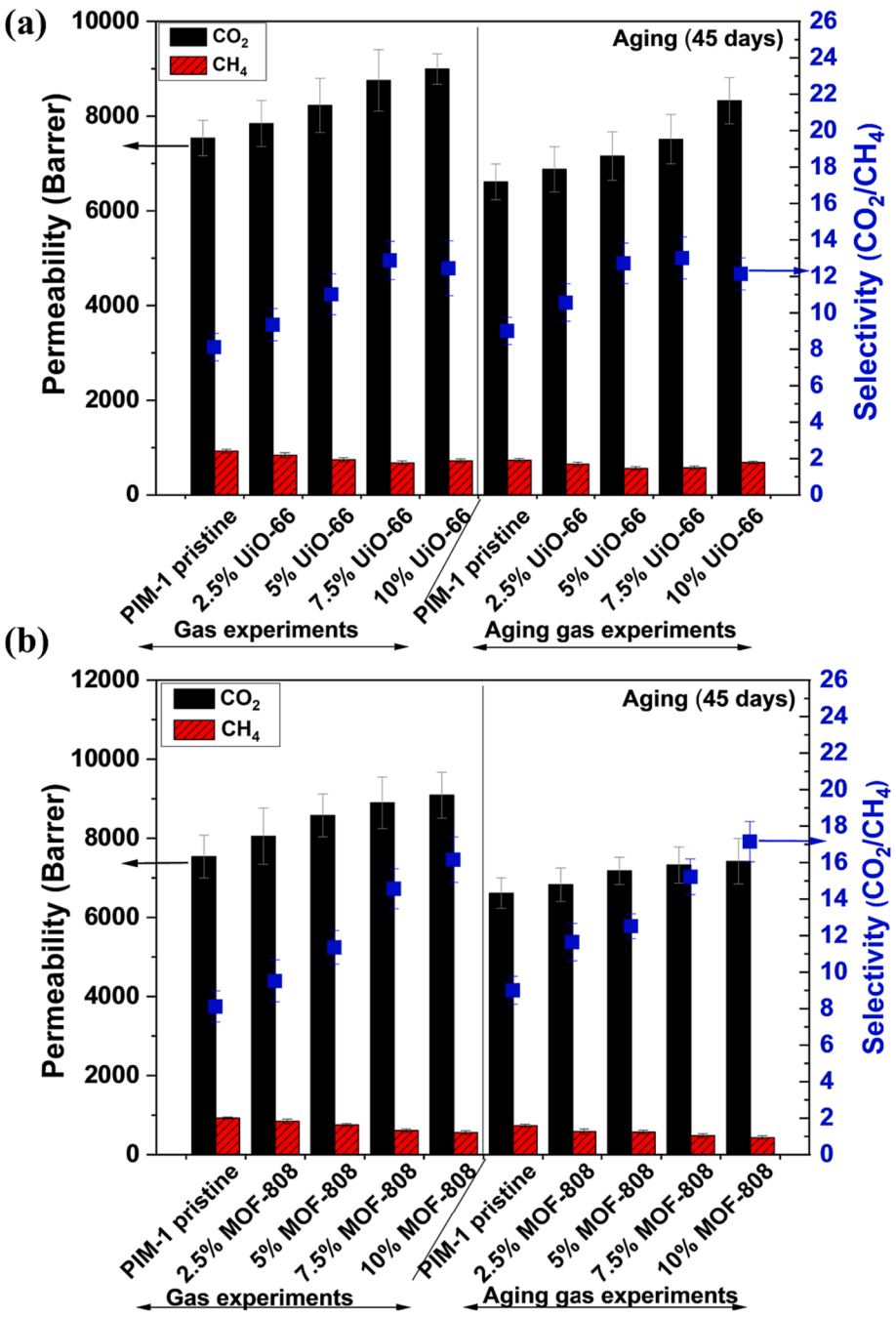

Fig. 6. CO_2 permeability and mixed (CO_2/CH_4) selectivity before and after aging (45 days) for: (a) PIM-1 pristine and PIM-1/UiO-66 MMMs; (b) PIM-1 and PIM-1/MOF-808 MMMs.

confirming a successful interaction between PIM-1 and the MOFs, but is not able to detect the mentioned UiO-66 agglomeration.

Furthermore, the mechanical strength of the synthesized membranes was assessed through a manual stretch test to evaluate their resistance and durability, this manual assessment indicated that the membrane exhibited favorable mechanical properties and strength (see Fig. S7 in the supplementary information for additional details).

3.2. *The separation performance for mixed gases*

The CO_2 permeabilities and CO_2/CH_4 selectivities of pristine PIM-1 and PIM-1/MOF MMMs are depicted in Table S2 and Figs. 6 and 7. The incorporation of MOF materials (UiO-66 and MOF-808) at varying loadings (2.5–10 wt%) had a noticeable influence on the performance of CO_2/CH_4 separation for PIM-1/MOF MMMs. Prior to aging, the inclusion of MOF particles in PIM-1 resulted in an improvement in the CO_2 permeability, increasing from approximately 7535 Barrer to a range of 7842–8995 Barrer for PIM-1/UiO-66 MMMs and to a range of 8052–9090 Barrer for PIM-1/MOF-808 MMMs. CO_2 permeabilities are higher when using MOF-808 as compared to UiO-66, in line with the larger porosity of the former. Additionally, the selectivity showed a rise from 8.1 to 12.5 for PIM-1/UiO-66 MMMs and from 8.1 to 16.2 for PIM-1/MOF-808, respectively, which can be attributed to the positive impact of incorporating UiO-66 and MOF-808 particles within the PIM-1 matrix, in agreement with the previous studies indicating that the porous property of the MOF nano-fillers improves gas permeability by facilitating the rate of gas diffusion [18,70,71].

Moreover, the results in Table S2 and Figs. 6 and 7 demonstrate the

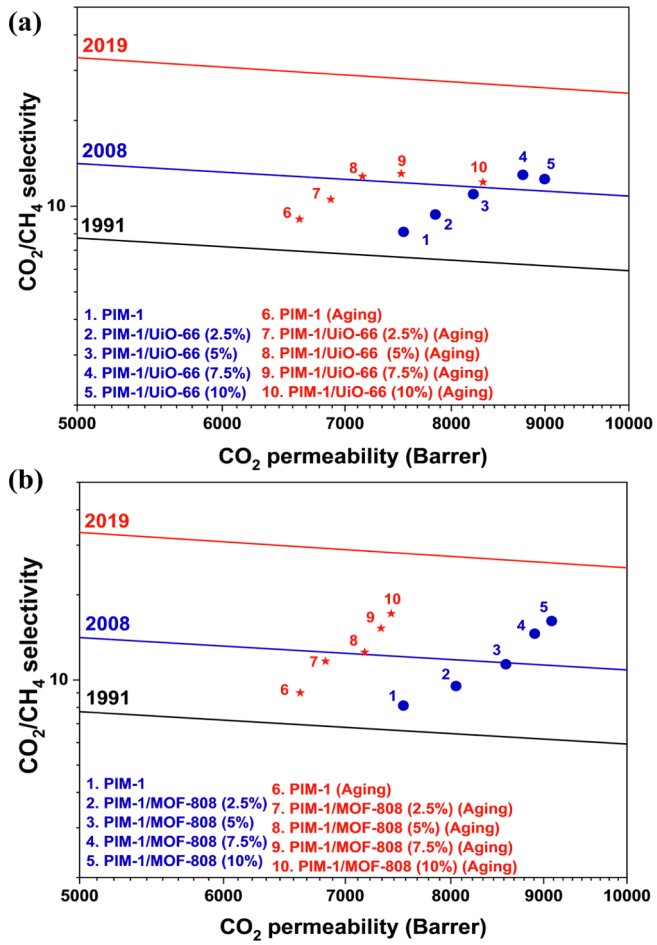

Fig. 7. Mixed (CO_2/CH_4) selectivity as a function of CO_2 permeability linked with the 1991 [4], 2008 [12] and 2019 [77] upper-bounds before and after aging for: (a) PIM-1 pristine and PIM-1/UiO-66 MMMs; (b) PIM-1 pristine and PIM-1/MOF-808 MMMs.

contrasting effects of incorporating MOF particles within the PIM-1 matrix membrane on the permeabilities of CO_2 and CH_4. CO_2 and CH_4 kinetic diameters are 0.33 nm and 0.38 nm, respectively, favoring the selective transport of the former. Moreover, this is enhanced through the microporous structure of the MOFs with pore sizes of ca. 0.6 and 1.8 nm for UiO-66 and MOF-808, respectively [43,55,56,59,72]. Indeed, it was observed that CO_2 molecules exhibited greater permeability through the PIM-1/MOF MMMs compared to CH_4 molecules. This phenomenon can also be attributed to the electrostatic interaction between the CO_2 quadrupole moment and the MOFs interaction sites [14,73,74], which enhances CO_2 permeability without showing specific interaction with CH_4. This is in line with the CO_2-philicity of both MOFs, with respective CO_2 adsorption capacities of 1.1 (25 °C, 100 kPa; 0.2 $mmol \cdot g^{-1}$ for CH_4 in the same conditions) and 1.3 $mmol \cdot g^{-1}$ (25 °C, 100 kPa) for UiO-66 [75] and MOF-808 [76], respectively, contribute to enhance the CO_2 solubility in the MMMs. This improves the CO_2/CH_4 separation selectivity, in line with previous observations in other PIM-1/MOF MMMs [14,73,74].

When evaluating the performance of gas separation for MMMs with various loading percentages of both MOFs (2.5–10 wt%), it is noticeable that the permeability gradually improves as the filler content increases (see Fig. 6a and Fig. 6b). This improvement is likely a consequence of the favorable diffusion pathway facilitated by pores present within the MOFs or at the interface between the MOF and the polymer matrix [11,14,35]. Moreover, as the loading percentage of MOF increases, there is a slight improvement in the CO_2/CH_4 selectivity (see Fig. 6a and Fig. 6b). Particularly noteworthy is the observation that incorporating Zr-based MOFs into the polymer matrix improves permeability and slightly selectivity [11,14,45]. This enhancement can be linked to the active functional groups present in the MOF ligands, which, besides the abovementioned CO_2-philic character, promote a stronger affinity between the MOF particles and PIM-1 [11,14,45]. Also, Fig. 7 illustrates that the MMMs with MOF loadings ranging from 5 to 10 wt% exhibit the most favorable separation performance, surpassing that of bare PIM-1 and even slightly exceeding the upper-bound Robeson line (2008) [5,12,77]. In terms of both CO_2 permeability (9090 Barrer) and CO_2/CH_4 separation selectivity (16.2), the best result was achieved with the 10 wt% PIM-1/MOF-808.

The physical aging characteristics of the tested membranes, encompassing bare PIM-1 and MMMs, were also evaluated. Following a duration of 45 days of aging (storing at room temperature in absence of light), a decline in CO_2 permeability and a slight enhance in CO_2/CH_4 selectivity were observed for all the MMMs (see Table S2 and Fig. 6). Previous research has highlighted that PIM-1, known for its high FFV, experiences physical aging, leading to a notable decrease in permeability over time along with a minor enhancement in selectivity [78–81]. This aging phenomenon is commonly observed in PIM-type polymers [82], where the polymer architecture gradually undergo local orientation/arrangement towards a pseudo-equilibrium state. This local orientation/arrangement results in a considerable reduction in FFV, thereby leading to a decline in membrane permeability with slight increase in selectivity [78–82]. Upon comparing the performance of the MMMs before and after aging, a consistent decline in permeability and an enhance in selectivity, following the upper-bounds, were observed. The upper-bound slope is only controlled by the kinetic diameter of diffused gas, and any variations along the slope demonstrate variations in diffusivity [3,4]. It is worthy notable that the aging primarily affects the properties of PIM-1 [14,18] as well as those of the PIM-1/MOFs MMMs undergoes significant aging processes in agreement with previous studies [83–85]. In any event, the aging in terms of CO_2 permeability decrease seems to follow this trend: PIM-1 (12% decrease) < PIM-1/UiO-66 MMMs (7–14 % decrease, with a remarkable low value of 7% decrease at the 10 wt% loading) < PIM-1/MOF-808 MMMs (15–18 % decrease). This is compensated with a general increase in CO_2/CH_4 selectivity following this trend: PIM-1/MOF-808 MMMs (4–23 % increase, the highest increase value of 23% being at the lowest loading of 2.5%) > PIM-1/UiO-66 MMMs (-3–15 % increase) > PIM-1 (11% decrease).

By comparing the performance of PIM-1/UiO-66 and PIM-1/MOF-808 MMMs, it is evident that all the MMMs demonstrated improved permeability and selectivity in comparison to the neat PIM-1, both before and after aging. However, PIM-1/MOF-808 MMMs demonstrated a higher level of separation performance compared to PIM-1/UiO-66 MMMs, particularly at the higher filler loadings of 7.5 and 10 wt%. Contrary to the expected due to the narrower porosity of UiO-66, the higher enhancement achieved with MOF-808 as compared to the bare polymer can be attributed to the better dispersibility and higher BET SSA of MOF-808 crystals in comparison to UiO-66 crystals. Indeed, the synthesis method for UiO-66 based on acetone instead of typical DMF produced a low BET SSA material. As mentioned before, the transport of gases through PIM-1, with varying pore volumes, pore sizes, and BET SSA values for the MOF crystals, can differ significantly due to the structural differences in PIM-1′s microporous network [63,65]. These variations play a crucial role in the improved performance observed in the PIM-1/MOF-808 MMMs. Additionally, the findings reveal a significant decline in CO_2/CH_4 selectivity for PIM-1/UiO-66 MMMs at the highest tested loading (10 wt%). This phenomenon was observed in other PIM-1/MOF MMMs as well. This can be demonstrated by the fact that the interactions between the polymer and filler materials create more twists and turns in the gas diffusion pathways, known as tortuosity. These interactions counterbalance the increased flexibility of the polymer chains, leading to an improved selectivity [18,70,71] up to a

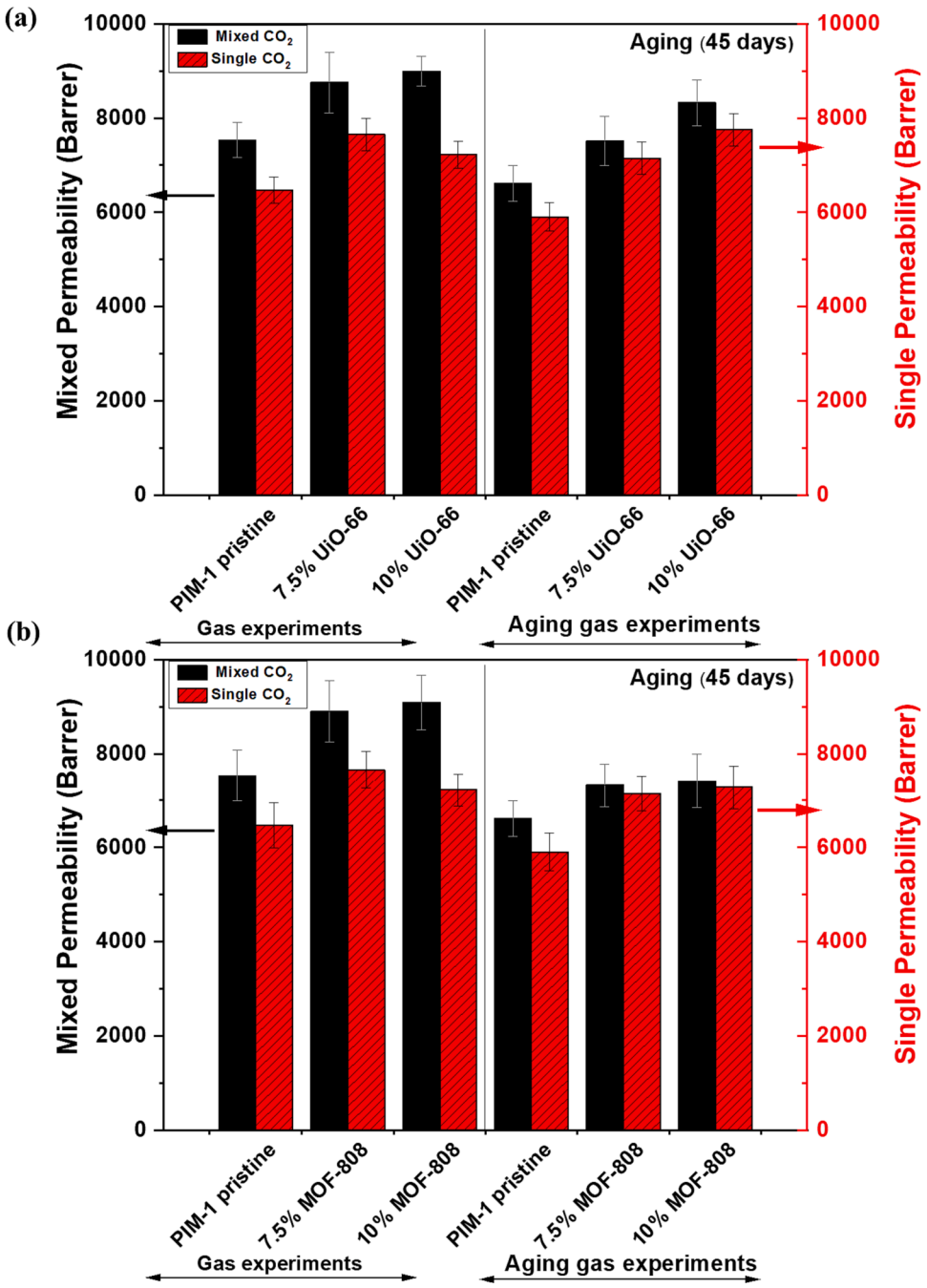

Fig. 8. CO_2 permeability for single and mixed gases before and after aging (45 days) for: (a) PIM-1 pristine and PIM-1/UiO-66 MMMs (7.5 and 10%); (b) PIM-1 and PIM-1/MOF-808 MMMs (7.5 and 10%).

certain level of MOF in the polymer. In fact, the non-uniform dispersion of MOF crystals results in a decline in FFV, impeding the efficiency of polymer chain disruption [14,18]. Therefore, the accumulation of UiO-66 within the PIM-1 matrix subsequently reduces the selectivity in PIM-1/UiO-66 (10 wt%), suggesting the 7.5 wt% loading as the optimum one. In contrast, this phenomenon was not observed in PIM-1/MOF-808 (10 wt%) MMMs, possibly due to the better MOF-PIM-1 interaction, reducing to some extension the mobility of the polymer architecture, and also to the homogeneous dispersion of MOF-808 (10 wt%) within the PIM-1. Besides being favored by the aging in terms of CO_2/CH_4 selectivity, these MOF-808 based MMMs exhibited the best separation performance in comparison to the pristine PIM-1 and the other MMMs based on UiO-66, amply surpassing the upper-bound line determined by Robeson (2008), as depicted in Fig. 7.

Furthermore, the single gas permeabilities of CO_2 and CH_4 were performed for the pristine PIM-1, PIM-1/UiO-66 (7.5 and 10 wt%), and PIM-1/MOF-808 MMMs (7.5 and 10 wt%), respectively, and the obtained results are compiled in Table S3 (Supplementary information) and Fig. 8 (permeabilities) and Fig. 9 (selectivities). Notably, mixed gases show higher CO_2 permeability and (CO_2/CH_4) selectivity compared to single gases [67,86–88]. This phenomenon is attributed to the microporous nature of PIM-1 membranes, allowing selective sorption and diffusion of gases based on their molecular size and polarity. In mixed gas environments, competition among gases with distinct properties occurs within the micropores, enhancing selectivity as the more permeable gas preferentially occupies these spaces, hindering less permeable gases [67,86–88]. Furthermore, interactions between different gas molecules in mixed gases lead to synergistic effects,

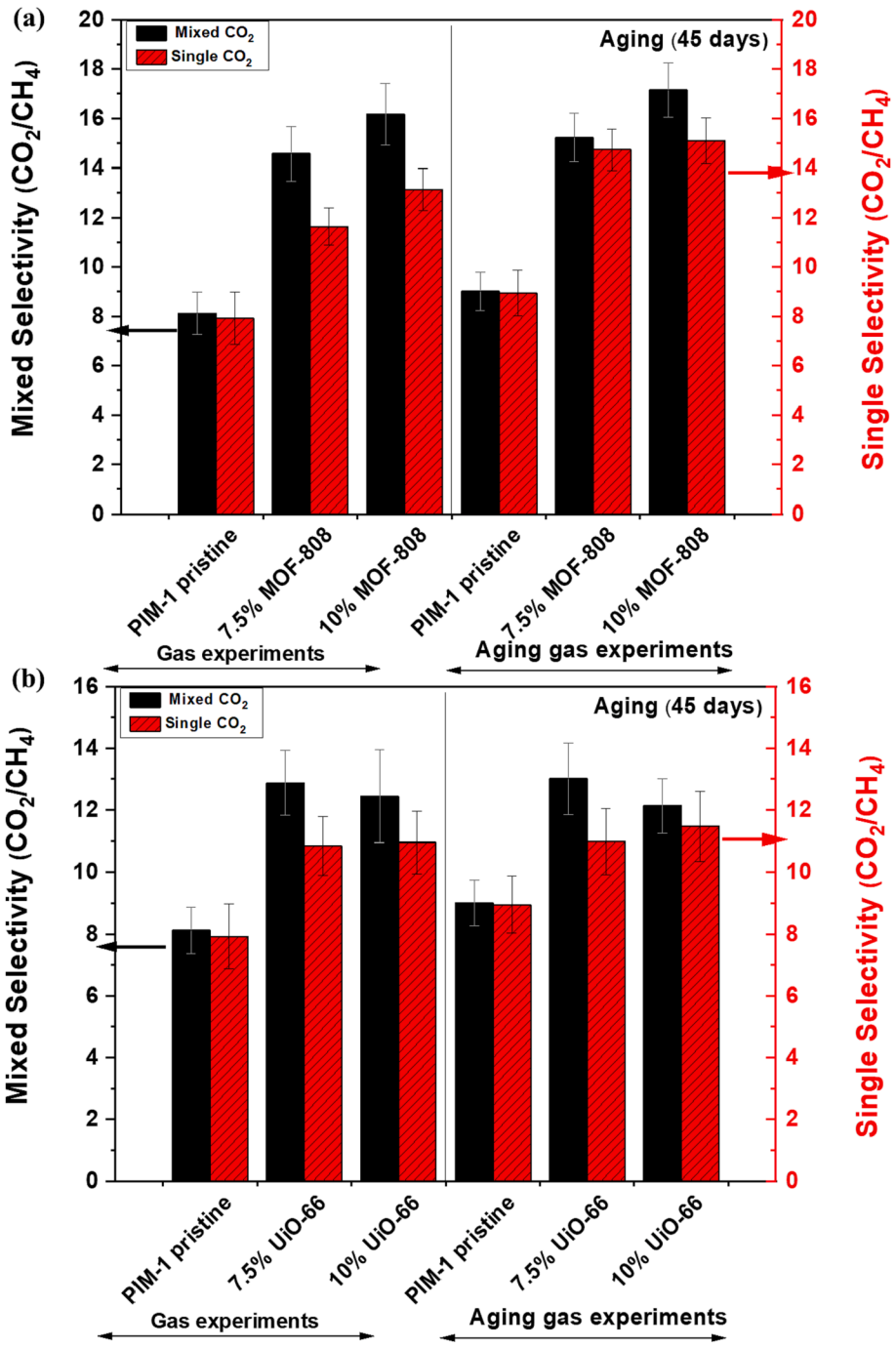

Fig. 9. (CO_2/CH_4) Selectivity for single and mixed gases before and after aging (45 days) for: (a) PIM-1 pristine and PIM-1/UiO-66 MMMs (7.5 and 10%); (b) PIM-1 and PIM-1/MOF-808 MMMs (7.5 and 10%).

resulting in increased overall permeability and selectivity compared to single gas scenarios. Overall, this study highlights the high potential of PIM-1/MOF MMMs as highly efficient materials for both mixed and single CO_2/CH_4 separation.

4. Conclusion

This study demonstrates the successful utilization of the sustainable microwave-assisted synthesis technique to fabricate MOFs UiO-66 and MOF-808 as fillers within a PIM-1 matrix for gas membrane separation. The resulting mixed matrix membranes (MMMs) exhibited notable enhancements in CO_2 permeability and CO_2/CH_4 selectivity in comparison to the PIM-1 pristine membrane. The improved performance can be associated to the porous nature of the two CO_2-philic MOFs, which facilitated enhanced gas diffusivity within the membranes. Higher loading of fillers resulted in even more favorable separation performance/efficiency, surpassing the Robeson upper-bound line (2008). Although aging of the MMMs led to a decline in CO_2 permeability, there was a remarkable increase in CO_2/CH_4 selectivity across all membranes. Despite these changes, the MMMs continued to outperform the pristine polymer membrane. Overall, this study highlights the high potential of PIM-1/MOF MMMs as highly efficient materials for mixed CO_2/CH_4 separation. The synthesis of nanosized MOFs UiO-66 and MOF-808 (with better result for MOF-808 in terms of crystallinity and BET SSA) and successful incorporation into PIM-1 yielded significant enhancements in CO_2 permeability and selectivity within the MMMs.

Summarizing the separation results with the two involved MOFs, the MOF-808 MMMs, besides being favored by the 45 days aging in terms of increased CO_2/CH_4 selectivity (up to 23% at 2.5 wt% filler loading), depicted the best separation performance in comparison to the pristine PIM-1 and the UiO-66 MMMs with a highest CO_2/CH_4 selectivity of 16.2 at a CO_2 permeability of 9090 Barrer at 10 wt% filler loading. These findings support an effective insight into the effects of MOF loading and aging on membrane performance, paving the way for further optimization and exploration of these MMMs in the field of sustainable gas separation technologies.

CRediT authorship contribution statement

Mohamed Yahia: Investigation, Conceptualization, Methodology, Visualization, Supervision, Writing – original draft, Writing – review & editing. **Luis A. Lozano:** Investigation, Methodology, Writing – original draft, Writing – review & editing. **Juan M. Zamaro:** Methodology, Writing – original draft, Writing – review & editing. **Carlos Téllez:** Conceptualization, Methodology, Visualization, Supervision, Funding acquisition, Writing – original draft, Writing – review & editing. **Joaquín Coronas:** Conceptualization, Methodology, Visualization, Supervision, Funding acquisition, Writing – original draft, Writing – review & editing.

Declaration of Competing Interest

The authors declare that they have no known competing financial interests or personal relationships that could have appeared to influence the work reported in this paper.

Data availability

Data will be made available on request.

Acknowledgments

This research acknowledges (TED2021-130621B-C41) grant supported by the European Union-NextGenerationEU, Ministerio de Ciencia e Innovación/MCIN, and the Spanish Agencia Estatal de Investigación/AEI. Also, the (PID2019-104009RB-I00) grant funded by (MCIN/AEI/10.13039/501100011033, AEI-MCIN, Spain). M. Yahia acknowledges the María Zambrano programme funding that supported by the Spanish Ministerio de Universidades and the European Union-NextGenerationEU. In addition, the authors thank the Aragón Government (T68_23R) financial support. Authors acknowledge at Universidad de Zaragoza (UNIZAR) (the Servicio General de Apoyo a la Investigación-SAI and the National Facility ELECMI ICTS, node Laboratorio de Microscopias Avanzadas) for the technical guides and instrumentation using. L.A. Lozano and J.M. Zamaro acknowledge the funding (Project PICT 1880) via the Agencia Nacional de Promoción Científica y Tecnológica of Argentina.

Appendix A. Supplementary data

Supplementary data to this article can be found online at https://doi.org/10.1016/j.seppur.2023.125558.

References

[1] Y. Zhang, J. Sunarso, S. Liu, R. Wang, Current status and development of membranes for CO_2/CH_4 separation: a review, Int. J. Greenhouse Gas Control 12 (2013) 84–107.
[2] H. Yang, Z. Xu, M. Fan, R. Gupta, R.B. Slimane, A.E. Bland, I. Wright, Progress in carbon dioxide separation and capture: a review, J. Environ. Sci. 20 (2008) 14–27.
[3] B.D. Freeman, Basis of permeability/selectivity tradeoff relations in polymeric gas separation membranes, Macromolecules 32 (1999) 375–380.
[4] L.M. Robeson, Correlation of separation factor versus permeability for polymeric membranes, J. Membr. Sci. 62 (1991) 165–185.
[5] L.M. Robeson, B.D. Freeman, D.R. Paul, B.W. Rowe, An empirical correlation of gas permeability and permselectivity in polymers and its theoretical basis, J. Membr. Sci. 341 (2009) 178–185.
[6] S. Basu, A.L. Khan, A. Cano-Odena, C. Liu, I.F.J. Vankelecom, Membrane-based technologies for biogas separations, Chem. Soc. Rev. 39 (2010) 750–768.
[7] X. Zou, G. Zhu, Microporous organic materials for membrane-based gas separation, Adv. Mater. 30 (2018) 1700750.
[8] R.W. Baker, B.T. Low, Gas separation membrane materials: a perspective, Macromolecules 47 (2014) 6999–7013.
[9] S. Wang, X. Li, H. Wu, Z. Tian, Q. Xin, G. He, D. Peng, S. Chen, Y. Yin, Z. Jiang, Advances in high permeability polymer-based membrane materials for CO_2 separations, Energ. Environ. Sci. 9 (2016) 1863–1890.
[10] G. Dong, H. Li, V. Chen, Challenges and opportunities for mixed-matrix membranes for gas separation, J. Mater. Chem. A 1 (2013) 4610–4630.
[11] M.R. Khdhayyer, E. Esposito, A. Fuoco, M. Monteleone, L. Giorno, J.C. Jansen, M. P. Attfield, P.M. Budd, Mixed matrix membranes based on UiO-66 MOFs in the polymer of intrinsic microporosity PIM-1, Sep. Purif. Technol. 173 (2017) 304–313.
[12] L.M. Robeson, The upper bound revisited, J. Membr. Sci. 320 (2008) 390–400.
[13] C.E. Powell, G.G. Qiao, Polymeric CO_2/N_2 gas separation membranes for the capture of carbon dioxide from power plant flue gases, J. Membr. Sci. 279 (2006) 1–49.
[14] M. Yahia, Q.N.P. Le, N. Ismail, M. Essalhi, O. Sundman, A. Rahimpour, M.M. Dal-Cin, N. Tavajohi, Effect of incorporating different ZIF-8 crystal sizes in the polymer of intrinsic microporosity, PIM-1, for CO_2/CH_4 separation, Microporous Mesoporous Mater. 312 (2021), 110761.
[15] T.-S. Chung, L.Y. Jiang, Y. Li, S. Kulprathipanja, Mixed matrix membranes (MMMs) comprising organic polymers with dispersed inorganic fillers for gas separation, Prog. Polym. Sci. 32 (2007) 483–507.
[16] N.A.H.M. Nordin, A.F. Ismail, A. Mustafa, R.S. Murali, T. Matsuura, Utilizing low ZIF-8 loading for an asymmetric PSf/ZIF-8 mixed matrix membrane for CO_2/CH_4 separation, RSC Adv. 5 (2015) 30206–30215.
[17] Y. Li, T.-S. Chung, C. Cao, S. Kulprathipanja, The effects of polymer chain rigidification, zeolite pore size and pore blockage on polyethersulfone (PES)-zeolite A mixed matrix membranes, J. Membr. Sci. 260 (2005) 45–55.
[18] D.-Y. Kang, J.S. Lee, Challenges in developing MOF-based membranes for gas separation, Langmuir 39 (2023) 2871–2880.
[19] C.A. Scholes, S. Kanehashi, Polymer of intrinsic microporosity (PIM-1) membranes treated with supercritical CO2, Membranes 9 (2019) 41.
[20] N.B. McKeown, P.M. Budd, Polymers of intrinsic microporosity (PIMs): organic materials for membrane separations, heterogeneous catalysis and hydrogen storage, Chem. Soc. Rev. 35 (2006) 675–683.
[21] N.B. McKeown, The structure-property relationships of Polymers of Intrinsic Microporosity (PIMs), Curr. Opin. Chem. Eng. 36 (2022), 100785.
[22] L. Hao, K.-S. Liao, T.-S. Chung, Photo-oxidative PIM-1 based mixed matrix membranes with superior gas separation performance, J. Mater. Chem. A 3 (2015) 17273–17281.
[23] M. Balçık, S.B. Tantekin-Ersolmaz, I. Pinnau, M.G. Ahunbay, CO_2/CH_4 mixed-gas separation in PIM-1 at high pressures: bridging atomistic simulations with process modeling, J. Membr. Sci. 640 (2021), 119838.
[24] P. Llewellyn, G. Maurin, J. Rouquerol, 14 - Adsorption by Metal-Organic Frameworks, in: F. Rouquerol, J. Rouquerol, K.S.W. Sing, P. Llewellyn, G. Maurin (Eds.), Adsorption by Powders and Porous Solids (Second Edition), Academic Press, Oxford, 2014, pp. 565–610.
[25] A. Karmakar, A.V. Desai, S.K. Ghosh, Ionic metal-organic frameworks (iMOFs): Design principles and applications, Coord. Chem. Rev. 307 (2016) 313–341.
[26] J.M. Luque-Alled, C. Moreno, P. Gorgojo, Two-dimensional materials for gas separation membranes, Curr. Opin. Chem. Eng. 39 (2023), 100901.
[27] E. Adatoz, A.K. Avci, S. Keskin, Opportunities and challenges of MOF-based membranes in gas separations, Sep. Purif. Technol. 152 (2015) 207–237.
[28] B. Zornoza, C. Tellez, J. Coronas, J. Gascon, F. Kapteijn, Metal organic framework based mixed matrix membranes: an increasingly important field of research with a large application potential, Microporous Mesoporous Mater. 166 (2013) 67–78.
[29] M. Rafiul Hasan, A. Moriones, M. Malankowska, J. Coronas, Study on the recycling of zeolitic imidazolate frameworks and polymer Pebax® 1657 from their mixed matrix membranes applied to CO_2 capture, Sep. Purif. Technol. 304 (2023), 122355.
[30] J.M. Luque-Alled, A.W. Ameen, M. Alberto, M. Tamaddondar, A.B. Foster, P. M. Budd, A. Vijayaraghavan, P. Gorgojo, Gas separation performance of MMMs containing (PIM-1)-functionalized GO derivatives, J. Membr. Sci. 623 (2021), 118902.
[31] Y. Feng, W. Yan, Z. Kang, X. Zou, W. Fan, Y. Jiang, L. Fan, R. Wang, D. Sun, Thermal treatment optimization of porous MOF glass and polymer for improving gas permeability and selectivity of mixed matrix membranes, Chem. Eng. J. 142873 (2023).
[32] L. Sze Lai, Y. Fong Yeong, K. Keong Lau, M., Shariff Az, Zeolite imidazole frameworks membranes for CO_2/CH_4 separation from natural gas: a review, J. Appl. Sci. 14 (2014) 1161–1167.
[33] E. Hernández-Marín, A.A. Lemus-Santana, Theoretical study of the formation of complexes between CO_2 and nitrogen heterocycles, J. Mex. Chem. Soc. 59 (2015) 36–42.
[34] D. Liu, Y. Wu, Q. Xia, Z. Li, H. Xi, Experimental and molecular simulation studies of CO_2 adsorption on zeolitic imidazolate frameworks: ZIF-8 and amine-modified ZIF-8, Adsorption 19 (2013) 25–37.

[35] N.A.H.M. Nordin, A.F. Ismail, A. Mustafa, R.S. Murali, T. Matsuura, The impact of ZIF-8 particle size and heat treatment on CO_2/CH_4 separation using asymmetric mixed matrix membrane, RSC Adv. 4 (2014) 52530–52541.
[36] A. Sabetghadam, B. Seoane, D. Keskin, N. Duim, T. Rodenas, S. Shahid, S. Sorribas, C.L. Guillouzer, G. Clet, C. Tellez, M. Daturi, J. Coronas, F. Kapteijn, J. Gascon, Metal organic framework crystals in mixed-matrix membranes: impact of the filler morphology on the gas separation performance, Adv. Funct. Mater. 26 (2016) 3154–3163.
[37] S. Hwang, W.S. Chi, S.J. Lee, S.H. Im, J.H. Kim, J. Kim, Hollow ZIF-8 nanoparticles improve the permeability of mixed matrix membranes for CO_2/CH_4 gas separation, J. Membr. Sci. 480 (2015) 11–19.
[38] S. Sorribas, B. Zornoza, C. Téllez, J. Coronas, Mixed matrix membranes comprising silica-(ZIF-8) core–shell spheres with ordered meso–microporosity for natural- and bio-gas upgrading, J. Membr. Sci. 452 (2014) 184–192.
[39] A.F. Bushell, M.P. Attfield, C.R. Mason, P.M. Budd, Y. Yampolskii, L. Starannikova, A. Rebrov, F. Bazzarelli, P. Bernardo, J. Carolus Jansen, M. Lanč, K. Friess, V. Shantarovich, V. Gustov, V. Isaeva, Gas permeation parameters of mixed matrix membranes based on the polymer of intrinsic microporosity PIM-1 and the zeolitic imidazolate framework ZIF-8, J. Membr. Sci. 427 (2013) 48–62.
[40] P. Tanvidkar, S. Appari, B.V.R. Kuncharam, A review of techniques to improve performance of metal organic framework (MOF) based mixed matrix membranes for CO_2/CH_4 separation, Rev. Environ. Sci. Bio/Technol. 21 (2022) 539–569.
[41] N.S. Hassan, A.A. Jalil, M.B. Bahari, N.F. Khusnun, E.M.S. Aldeen, R.S. Mim, M. L. Firmansyah, S. Rajendran, R.R. Mukti, R. Andika, H. Devianto, A comprehensive review on zeolite-based mixed matrix membranes for CO_2/CH_4 separation, Chemosphere 314 (2023), 137709.
[42] O.G. Nik, X.Y. Chen, S. Kaliaguine, Functionalized metal organic framework-polyimide mixed matrix membranes for CO_2/CH_4 separation, J. Membr. Sci. 413–414 (2012) 48–61.
[43] Q. Yang, A.D. Wiersum, P.L. Llewellyn, V. Guillerm, C. Serre, G. Maurin, Functionalizing porous zirconium terephthalate UiO-66(Zr) for natural gas upgrading: a computational exploration, Chem. Commun. 47 (2011) 9603–9605.
[44] D. Wu, G. Maurin, Q. Yang, C. Serre, H. Jobic, C. Zhong, Computational exploration of a Zr-carboxylate based metal–organic framework as a membrane material for CO_2 capture, J. Mater. Chem. A 2 (2014) 1657–1661.
[45] N. Tien-Binh, D. Rodrigue, S. Kaliaguine, In-situ cross interface linking of PIM-1 polymer and UiO-66-NH2 for outstanding gas separation and physical aging control, J. Membr. Sci. 548 (2018) 429–438.
[46] L. Jiang, Y. Dong, Y. Yuan, X. Zhou, Y. Liu, X. Meng, Recent advances of metal–organic frameworks in corrosion protection: From synthesis to applications, Chem. Eng. J. 430 (2022), 132823.
[47] M.D. Guiver, M. Yahia, M.M. Dal-Cin, G.P. Robertson, S. Saeedi Garakani, N. Du, N. Tavajohi, Gas transport in a polymer of intrinsic microporosity (PIM-1) substituted with pseudo-ionic liquid tetrazole-type structures, Macromolecules 53 (2020) 8951–8959.
[48] L.A. Lozano, C.M. Iglesias, B.M.C. Faroldi, M.A. Ulla, J.M. Zamaro, Efficient solvothermal synthesis of highly porous UiO-66 nanocrystals in dimethylformamide-free media, J. Mater. Sci. 53 (2018) 1862–1873.
[49] L.A. Lozano, A. Devard, M.A. Ulla, J.M. Zamaro, Cu/UiO-66: a novel nanocatalyst obtained by a microwave-assisted protocol in DMF-free media for the efficient phenol removal via catalytic wet peroxide oxidation, J. Environ. Chem. Eng. 8 (2020), 104332.
[50] H. Reinsch, S. Waitschat, S.M. Chavan, K.P. Lillerud, N. Stock, A. Facile, "Green" route for scalable batch production and continuous synthesis of zirconium MOFs, Eur. J. Inorg. Chem. 2016 (2016) 4490–4498.
[51] M.Z. Ahmad, T.A. Peters, N.M. Konnertz, T. Visser, C. Téllez, J. Coronas, V. Fila, W. M. de Vos, N.E. Benes, High-pressure CO_2/CH_4 separation of Zr-MOFs based mixed matrix membranes, Sep. Purif. Technol. 230 (2020), 115858.
[52] Y. Cheng, Y. Ying, L. Zhai, G. Liu, J. Dong, Y. Wang, M.P. Christopher, S. Long, Y. Wang, D. Zhao, Mixed matrix membranes containing MOF@COF hybrid fillers for efficient CO_2/CH_4 separation, J. Membr. Sci. 573 (2019) 97–106.
[53] J.H. Cavka, S. Jakobsen, U. Olsbye, N. Guillou, C. Lamberti, S. Bordiga, K. P. Lillerud, A new zirconium inorganic building brick forming metal organic frameworks with exceptional stability, J. Am. Chem. Soc. 130 (2008) 13850–13851.
[54] H. Furukawa, F. Gándara, Y.-B. Zhang, J. Jiang, W.L. Queen, M.R. Hudson, O. M. Yaghi, Water adsorption in porous metal-organic frameworks and related materials, J. Am. Chem. Soc. 136 (2014) 4369–4381.
[55] Z. Li, W. Zhang, M. Tao, L. Shen, R. Li, M. Zhang, Y. Jiao, H. Hong, Y. Xu, H. Lin, In-situ growth of UiO-66-NH2 in porous polymeric substrates at room temperature for fabrication of mixed matrix membranes with fast molecular separation performance, Chem. Eng. J. 435 (2022), 134804.
[56] L.A. Lozano, L.A.S. Hoyos, B.M.C. Faroldi, J.M. Zamaro, Enhancement in the CO_2 uptake of UiO-66 by a simple exposure to ultraviolet light, Mater. Today Commun. 31 (2022), 103540.
[57] G. Morales, M. Paniagua, D. de la Flor, M. Sanz, P. Leo, C. López-Aguado, H. Hernando, S.A. Orr, K. Wilson, A.F. Lee, J.A. Melero, Aldol condensation of furfural and methyl isobutyl ketone over Zr-MOF-808/silica hybrid catalysts, Fuel 339 (2023), 127465.
[58] C. Ardila-Suárez, A.M. Díaz-Lasprilla, L.A. Díaz-Vaca, P.B. Balbuena, V. G. Baldovino-Medrano, G.E. Ramírez-Caballero, Synthesis, characterization, and post-synthetic modification of a micro/mesoporous zirconium–tricarboxylate metal–organic framework: towards the addition of acid active sites, J CrystEngComm 21 (2019) 3014–3030.
[59] L. Valenzano, B. Civalleri, S. Chavan, S. Bordiga, M.H. Nilsen, S. Jakobsen, K. P. Lillerud, C. Lamberti, Disclosing the complex structure of UiO-66 metal organic framework: a synergic combination of experiment and theory, Chem. Mater. 23 (2011) 1700–1718.
[60] M. Lammert, C. Glißmann, N. Stock, Tuning the stability of bimetallic Ce(iv)/Zr (iv)-based MOFs with UiO-66 and MOF-808 structures, Dalton Trans. 46 (2017) 2425–2429.
[61] P.M. Budd, B.S. Ghanem, S. Makhseed, N.B. McKeown, K.J. Msayib, C. E. Tattershall, Polymers of intrinsic microporosity (PIMs): robust, solution-processable, organic nanoporous materials, Chem. Commun. (2004) 230–231.
[62] N.B. McKeown, P.M. Budd, K.J. Msayib, B.S. Ghanem, H.J. Kingston, C. E. Tattershall, S. Makhseed, K.J. Reynolds, D. Fritsch, Polymers of intrinsic microporosity (PIMs): bridging the void between microporous and polymeric materials, Chem. –Eur. J. 11 (2005) 2610–2620.
[63] N.B. McKeown, Polymers of intrinsic microporosity (PIMs), Polymer 202 (2020), 122736.
[64] M. Tian, S. Rochat, H. Fawcett, A.D. Burrows, C.R. Bowen, T.J. Mays, Chemical modification of the polymer of intrinsic microporosity PIM-1 for enhanced hydrogen storage, Adsorption 26 (2020) 1083–1091.
[65] K. Chen, S.H. Mousavi, R. Singh, R.Q. Snurr, G. Li, P.A. Webley, Gating effect for gas adsorption in microporous materials—mechanisms and applications, Chem. Soc. Rev. 51 (2022) 1139–1166.
[66] Z. Zhao, H. Li, K. Zhao, L. Wang, X. Gao, Microwave-assisted synthesis of MOFs: Rational design via numerical simulation, Chem. Eng. J. 428 (2022), 131006.
[67] S. He, B. Zhu, S. Li, Y. Zhang, X. Jiang, C.H. Lau, L. Shao, Recent progress in PIM-1 based membranes for sustainable CO_2 separations: Polymer structure manipulation and mixed matrix membrane design, Sep. Purif. Technol. 284 (2022), 120277.
[68] K. Polak-Kraśna, R. Dawson, L.T. Holyfield, C.R. Bowen, A.D. Burrows, T.J. Mays, Mechanical characterisation of polymer of intrinsic microporosity PIM-1 for hydrogen storage applications, J. Mater. Sci. 52 (2017) 3862–3875.
[69] A.R. Nabais, A.P.S. Martins, V.D. Alves, J.G. Crespo, I.M. Marrucho, L.C. Tomé, L. A. Neves, Poly(ionic liquid)-based engineered mixed matrix membranes for CO2/H2 separation, Sep. Purif. Technol. 222 (2019) 168–176.
[70] J. Sánchez-Laínez, A. Pardillos-Ruiz, M. Carta, R. Malpass-Evans, N.B. McKeown, C. Téllez, J. Coronas, Polymer engineering by blending PIM-1 and 6FDA-DAM for ZIF-8 containing mixed matrix membranes applied to CO_2 separations, Sep. Purif. Technol. 224 (2019) 456–462.
[71] N. Tien-Binh, H. Vinh-Thang, X.Y. Chen, D. Rodrigue, S. Kaliaguine, Crosslinked MOF-polymer to enhance gas separation of mixed matrix membranes, J. Membr. Sci. 520 (2016) 941–950.
[72] W. Liang, H. Chevreau, F. Ragon, P.D. Southon, V.K. Peterson, D.M. D'Alessandro, Tuning pore size in a zirconium–tricarboxylate metal–organic framework, CrstEngComm 16 (2014) 6530–6533.
[73] Z.R. Herm, J.A. Swisher, B. Smit, R. Krishna, J.R. Long, Metal−organic frameworks as adsorbents for hydrogen purification and precombustion carbon dioxide capture, J. Am. Chem. Soc. 133 (2011) 5664–5667.
[74] Z. Bao, S. Alnemrat, L. Yu, I. Vasiliev, Q. Ren, X. Lu, S. Deng, Kinetic separation of carbon dioxide and methane on a copper metal–organic framework, J. Colloid Interface Sci. 357 (2011) 504–509.
[75] S. Mutyala, M. Jonnalagadda, S.M. Ibrahim, Effect of modification of UiO-66 for CO_2 adsorption and separation of CO_2/CH_4, J. Mol. Struct. 1227 (2021), 129506.
[76] H.J. Jun, D.K. Yoo, S.H. Jhung, Metal-organic framework (MOF-808) functionalized with ethyleneamines: selective adsorbent to capture CO2 under low pressure, J. CO_2 Util. 58 (2022), 101932.
[77] B. Comesaña-Gándara, J. Chen, C.G. Bezzu, M. Carta, I. Rose, M.-C. Ferrari, E. Esposito, A. Fuoco, J.C. Jansen, N.B. McKeown, Redefining the Robeson upper bounds for CO_2/CH_4 and CO_2/N_2 separations using a series of ultrapermeable benzotriptycene-based polymers of intrinsic microporosity, Energ. Environ. Sci. 12 (2019) 2733–2740.
[78] P. Bernardo, F. Bazzarelli, F. Tasselli, G. Clarizia, C.R. Mason, L. Maynard-Atem, P. M. Budd, M. Lanč, K. Pilnáček, O. Vopička, K. Friess, D. Fritsch, Y.P. Yampolskii, V. Shantarovich, J.C. Jansen, Effect of physical aging on the gas transport and sorption in PIM-1 membranes, Polymer 113 (2017) 283–294.
[79] S. Harms, K. Rätzke, F. Faupel, N. Chaukura, P.M. Budd, W. Egger, L. Ravelli, Aging and free volume in a polymer of intrinsic microporosity (PIM-1), J. Adhes. 88 (2012) 608–619.
[80] R. Swaidan, B. Ghanem, E. Litwiller, I. Pinnau, Physical aging, plasticization and their effects on gas permeation in "Rigid" polymers of intrinsic microporosity, Macromolecules 48 (2015) 6553–6561.
[81] R.R. Tiwari, J. Jin, B.D. Freeman, D.R. Paul, Physical aging, CO_2 sorption and plasticization in thin films of polymer with intrinsic microporosity (PIM-1), J. Membr. Sci. 537 (2017) 362–371.
[82] R. Swaidan, B. Ghanem, M. Al-Saeedi, E. Litwiller, I. Pinnau, Role of intrachain rigidity in the plasticization of intrinsically microporous triptycene-based polyimide membranes in mixed-gas CO_2/CH_4 separations, Macromolecules 47 (2014) 7453–7462.
[83] C. Geng, Y. Sun, Z. Zhang, Z. Qiao, C. Zhong, mitigated aging in a defective metal-organic framework pillared polymer of an intrinsic porosity hybrid membrane for efficient gas separation, ACS Sustain. Chem. Eng. 10 (2022) 3643–3650.
[84] K. Chen, L. Ni, H. Zhang, C. Xiao, L. Li, X. Guo, J. Qi, C. Wang, X. Sun, J. Li, Incorporating KAUST-7 into PIM-1 towards mixed matrix membranes with long-term stable CO_2/CH_4 separation performance, J. Membr. Sci. 661 (2022), 120848.
[85] E. Aliyev, J. Warfsmann, B. Tokay, S. Shishatskiy, Y.-J. Lee, J. Lillepaerg, N. R. Champness, V. Filiz, Gas transport properties of the metal–organic framework (MOF)-assisted polymer of intrinsic microporosity (PIM-1) thin-film composite membranes, ACS Sustain. Chem. Eng. 9 (2020) 684–694.

[86] S. Thomas, I. Pinnau, N. Du, M.D. Guiver, Pure- and mixed-gas permeation properties of a microporous spirobisindane-based ladder polymer (PIM-1), J. Membr. Sci. 333 (2009) 125–131.
[87] A.E. Gemeda, M.G. De Angelis, N. Du, N. Li, M.D. Guiver, G.C. Sarti, Mixed gas sorption in glassy polymeric membranes. III. CO2/CH4 mixtures in a polymer of intrinsic microporosity (PIM-1): Effect of temperature, J. Membr. Sci. 524 (2017) 746–757.
[88] L. Martínez-Izquierdo, A. Perea-Cachero, M. Malankowska, C. Téllez, J. Coronas, A comparative study between single gas and mixed gas permeation of polyether-block-amide type copolymer membranes, J. Environ. Chem. Eng. 10 (2022), 108324.